Numerical Simulation of a Pool Fire

Dong-Eun Lee* and Seung-Wook Baek**

(*Received November 14, 1997*)

Thermo-fluid mechanical characteristics as well as flame structure of a pool fire were numerically simulated in this study. The small scale pool fire was treated as a gaseous jet flame with low initial velocity as an approximation. The combustion model postulated infinitely fast chemical reaction and the soot formation model included soot nucleation, surface growth, coagulation, thermophoresis, and oxidation. Valuable data were obtained in the temperature distribution, velocity profiles, soot volume fraction and major species concentrations. Especially, the periodic formation of the large scale structures were successfully simulated. Its frequency agreed well with experimental results.

Key Words: Pool Fire, Oscillation Frequency, Scale Effect

Nomenclature

a : Absorption coefficient
c_v : Specific heat at constant volume
E : Energy density
f_v : Soot volume fraction
g : Gravitational acceleration
h_k : Enthalpy of species k
I_b : Blackbody intensity
k : Boltzmann constant
n : Total species number density
n_d : Soot number density
n_k : Number density of species k
P_{o_2} : Partial pressure of oxygen
q_c : Thermal conductive heat flux
q_r : Radiative heat flux
T : Temperature
$\vec{v}$: Fluid velocity
$\vec{v_k}$: Diffusion velocity
X_k : Mole fraction of species k
ν : Kinematic viscosity
τ : Viscous stress tensor
Ω : Direction of radiation
ω_{f_v} : Production or loss of soot volume fraction
ω_{n_d} : Production or loss of soot number density

* Research Institute of Industrial Science and Technology, Heat and Fluid Flow Research Team
** Korea Advanced Institute of Science and Technology, Aerospace Engineering Department

1. Introduction

Fires over horizontal fuel surfaces are called pool fires and are used as models of freely burning fires in their early stages of development. Because combustion and heat transfer in the pool fires primarily occur in the vapor phase, the flames above flat gas burners may be exploited for theoretical modeling as well as experimental investigations in freely burning actual fire or pool fire research. The gas flames which qualify for such a study must be buoyant diffusion flames. Considering a flame above a burning horizontal surface, the Froude number is defined as :

$$F_o = V_{z_o}/gD \tag{1}$$

where V_{z_o} is the initial vertical velocity of the gas and D is the characteristic length of the gas flux. At standard conditions of pressure and temperature, these buoyant diffusion flames possess low Froude numbers and typical values are in the range :

$$10^{-6} \leq F_o \leq 10^{-4} \tag{2}$$

Of most importance, pool fires exhibit a periodic oscillatory motion, also known as the flame flicker. Figure 1 summarizes flame oscillation or the outer-vortex occurrence and passing fre-

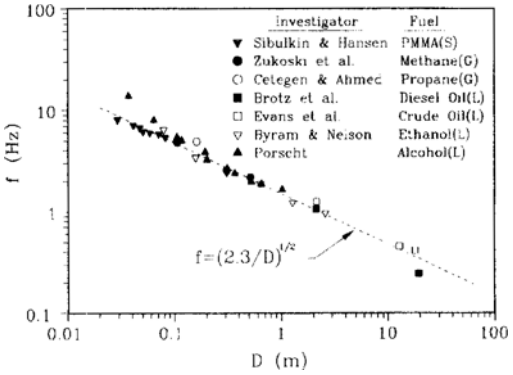

Fig. 1 Measured oscillation frequencies as a function of burner diameter.

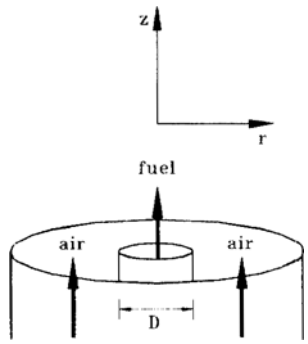

Fig. 2 Schematic of geometry.

quency as a function of source diameter of fire from many investigations. The oscillation frequency shows a definite trend with flame base diameter and $f^2 \simeq 2.3/D$ describes the frequency over more than three order of magnitude of the flame base diameter from 0.02 to 20m. The flame oscillation frequency appears to be uninfluenced by the fuel type as indicated by the data of Fig. 1.

In this study, we numerically simulate gaseous fuel, small-scale pool fires. In particular, the present study will simulate buoyant flames using ethylene as fuel and investigate the large-scale structures that are experimentally observed, as well as the detailed calculation of flame properties.

2. Numerical Model

A schematic of the geometry is shown in Fig. 2. The fuel (ethylene) exits upward from a vertically oriented tube of diameter D with a uniformly distributed velocity and the coflowing air stream is unconfined. The resulting buoyant flame is substantially axisymmetric, thus requiring only the radial (r) and axial (z) coordinates in order to uniquely define a point. The species considered in the model (C_2H_4, O_2, N_2, CO_2, and H_2O) are assumed to be ideal gases.

The computer code solves the time-dependent equations for conservation of mass density, momentum, energy, individual species number densities, soot number density, and soot volume fraction. The governing conservation equations are shown below.

$$\frac{\partial \rho}{\partial t} + \nabla \cdot (\rho \vec{v}) = 0 \tag{3}$$

$$\frac{\partial \rho \vec{v}}{\partial t} + \nabla \cdot (\rho \vec{v} \vec{v}) = -\nabla P + \rho \vec{g} - \nabla \cdot \tau \tag{4}$$

$$\frac{\partial E}{\partial t} + \nabla \cdot (E \vec{v}) = -\nabla \cdot P \vec{v} - \nabla \cdot (q_c + q_r) - \nabla \cdot \sum n_k \vec{v}_k h_k + Q \tag{5}$$

$$\frac{\partial n_k}{\partial t} + \nabla \cdot (n_k \vec{v}) = -\nabla \cdot (n_k \vec{v}_k) + \omega_k \tag{6}$$

$$\frac{\partial n_d}{\partial t} + \nabla \cdot (n_d \vec{v}) = -\nabla \cdot (\vec{v}_t n_d) + \omega_{n_d} \tag{7}$$

$$\frac{\partial f_v}{\partial t} + \nabla \cdot (f_v \vec{v}) = -\nabla \cdot (\vec{v}_t f_v) + \omega_{f_v} \tag{8}$$

The solution to the fluid convective terms in Eqs. (3) ~ (8) is obtained using Barely Implicit Correction to Flux Corrected Transport (BIC-FCT). The diffusive transport processes included in this model are molecular diffusion, thermal conduction and viscosity, all processes that are important physical phenomena for describing flame structure.

The energy source term, Q, in Eq. (5) is principally due to the heat produced by chemical reaction, and the production and loss of species are represented by the source term, ω_k, in Eq. (6). A simple chemical model is used for ethylene oxidation in which fuel, oxidizer, products and inert gas (N_2) are assumed to undergo a single, global reaction step given as :

$$C_2H_4 + 3O_2 \rightarrow 2CO_2 + 2H_2O \tag{9}$$

At the fuel-oxygen interface, chemical reaction is assumed to be infinitely fast.

The conservation equations for soot number density and volume fraction, Eqs. (7) ~ (8),

include source terms, ω_{n_d} and ω_{f_v}. These source terms are represented by two coupled ordinary differential equations based on the experimental measurements by Moss et al. (1988) :

$$\omega_{n_d}=1.0234\times10^{32}\rho^2T^{1/2}X_{fuel}e^{-46100/T}-1.6611\times10^{-9}T^{1/2}n_d^2 \quad (10)$$

$$\omega_{f_v}=2.333\times10^{-11}n_d\rho T^{1/2}X_{fuel}e^{-12600/T}+1.36\times10^{13}\rho^2T^{1/2}X_{fuel}e^{-46100/T} \quad (11)$$

where the soot particle density of spherical shape is assumed to be 1.8 g/cm^3. This model sought to include the influences of soot nucleation, surface growth and coagulation on the soot formation rate. The soot oxidation rate, R_{ox}, is calculated by the expression of Nagle et al. (1962) and these rate are then subtracted from the right-hand side of Eq. (10) and Eq. (11), so that these source terms include the additional effect of soot oxidation.

$$R_{ox}=12\left[\left(\frac{k_AP_{o_2}}{1+k_ZP_{o_2}}\right)\chi+k_BP_{o_2}(1-\chi)\right] \quad (12)$$

where

$$\chi=[1+k_T/(k_BP_{o_2})]^{-1}$$
$$k_A=20\ \exp(-30000/RT)$$
$$k_B=4.46\times10^{-3}\exp(-15200/RT)$$
$$k_T=1.51\times10^5\ \exp(-97000/RT)$$
$$k_Z=21.3\ \exp(4100/RT)$$

Soot particles are convected along gas flow, but also drift in the radial direction due to thermophoretic forces arising from the temperature gradients. Equations (7) and (8) also include thermo-phoresis term to the soot particles, and consider only the radial component of this effect, where the thermophoretic velocity, $\vec{v}_t$, is defined by Moss et al. (1988) :

$$\vec{v}_t=-0.54\nu\frac{\partial\ln T}{\partial r} \quad (13)$$

The effect of radiation transport appears in energy conservation equation as the divergence of the radiative heat flux :

$$-\nabla\cdot q_r=a(r)\left[\int_{4\pi}I(r,\ \Omega)\,d\Omega-4\pi I_b\right] \quad (14)$$

To find the directional intensity, $I(r,\ \Omega)$, radiative transfer equation for gray gases is solved using the Discrete Ordinate Method (DOM) and the effect of scattering is neglected. The absorption coefficient for soot which are used in this calculation is that from Kent and Honnery (1990) :

$$a_{soot}=2.66const.\ f_vT \quad (15)$$

where const.=7, and absorption coefficient for the mixture of H_2O and CO_2 that from Magnussen and Hjertager (1977) :

$$a_{CO_2+H_2O}=0.001(X_{CO_2}+X_{H_2O}) \quad (16)$$

They are summed to obtain an overall absorption coefficient for each cell.

3. Model Validation

In order to validate the present model, we simulated a low-speed buoyant diffusion flame and compared the predicted results with experimental data of Santoro et al. (1987). The experimental burner of Santoro et al. consisted of an 1.11cm i. d. fuel passage surrounded by a 10.16cm concentric outer air passage. We obtained the velocity and temperature data over a period of 0.7 second and averaged for comparison with their experimental results.

In Fig. 3, we compared the computed centerline axial velocities with the measured data and a reasonably good agreement is observed between them. From Fig. 3, we can see that the effects of buoyancy are not dominant at the flame base, but the gases along the centerline are accelerated by the prevailing buoyant forces with height.

Comparison of radial temperature profiles are shown in Fig. 4. In the lower part of the flame

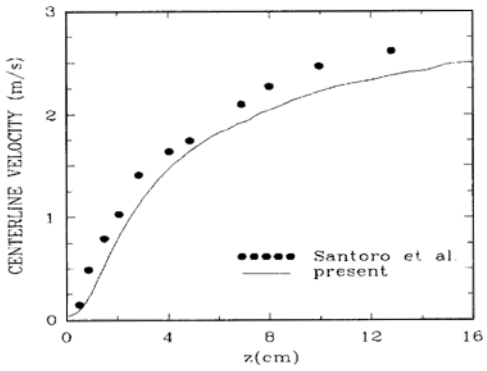

Fig. 3 Comparison between simulation and experimental result in the centerline axial velocity.

(Fig. 4-(a), (b)), the simulations underpredict the temperature close to the centerline. This may be due to not including the nozzle itself in the computational domain. However, with increasing radial distance from the flame axis and increasing height, the agreement is quite good.

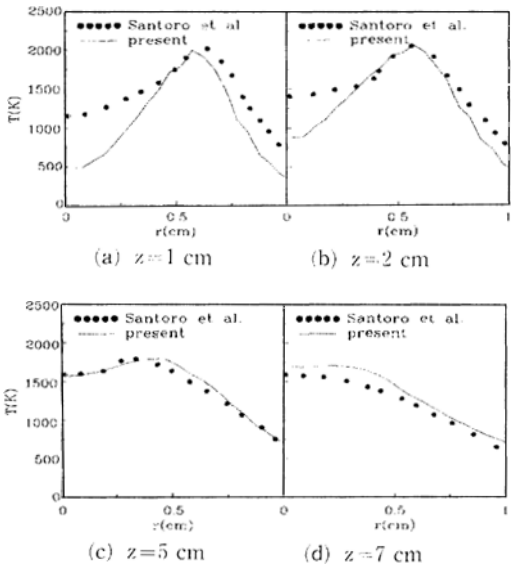

Fig. 4 Comparison of radial temperature distribution at various heights. (z=1, 2, 5, 7cm)

4. Results and Discussion

First, computations have been carried out with the conditions of Flame I. Simulation conditions

Table 1 Summary of simulation conditions.

Properties	Flame I	Flame II	Flame III
Burner diameter (m)	0.02	0.05	0.10
Burner exit velocity of fuel (m/s)	0.02	0.02	0.02
Heat release rate (kW)	0.36	2.26	9.03
Fuel flow rate (kg/s)	7.16e-6	4.48e-5	1.79e-4
Burner exit Froude number	2.04e-6	8.16e-4	4.08e-4
Burner exit temperature (K)	298	298	298

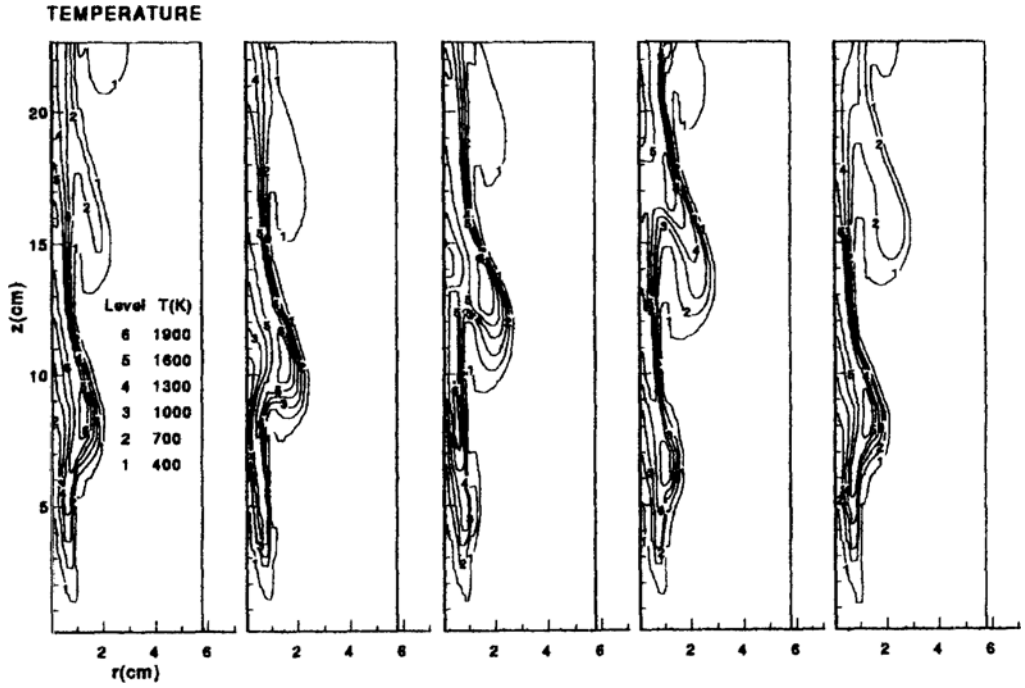

Fig. 5 Time-sequence of selected temperature contours from time step 20000 for case of Flame I. The time interval between frames is 30ms.

are shown in Table 1.

Figure 5 shows a time sequence of the selected temperature contours of the computed flame. As can be seen, this method correctly describes large -scale, time dependent processes involving buoyancy and large density variations. In the first frame, a bulge is developing and it slowly moves downstream in subsequent frames. In the final frame, it is moving out of the domain shown as the next instability forms below it. The frequency range of 10-11Hz associated with the motion of these large vortices compares well with the experimental value (10.5Hz) from Fig. 1.

The instantaneous radial temperature distributions at various axial heights are shown in Fig. 6. The width of profile is narrow nearest the burner exit (z=4cm). At the next higher axial location, the profile becomes broader as the flame starts to bulge outward. In the contraction region at the next height, they narrow again. At the highest location indicated (z=13cm), double peaks appear just below the large-scale structure and this is believed to be due to the entrainment of hot gases into the large vortex. The outer structures become weaker and move out of the domain. The maximum temperature, about 2020K, is located at r=1.2cm, z=7.5cm.

Figure 7 shows the instantaneous contours of unburned fuel mole fraction, O_2 mole fraction, combustion products (H_2O, CO_2) mole fraction, and soot volume fraction at time step 20000.The maxima in the water vapor and carbon dioxide

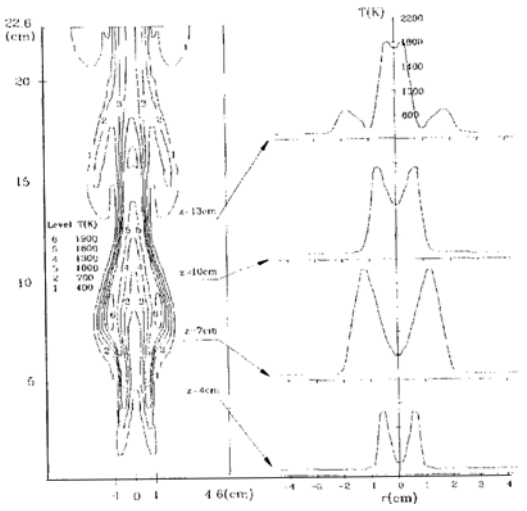

Fig. 6 Instantaneous radial temperature distribution at time step 20000 for case of Flame I.

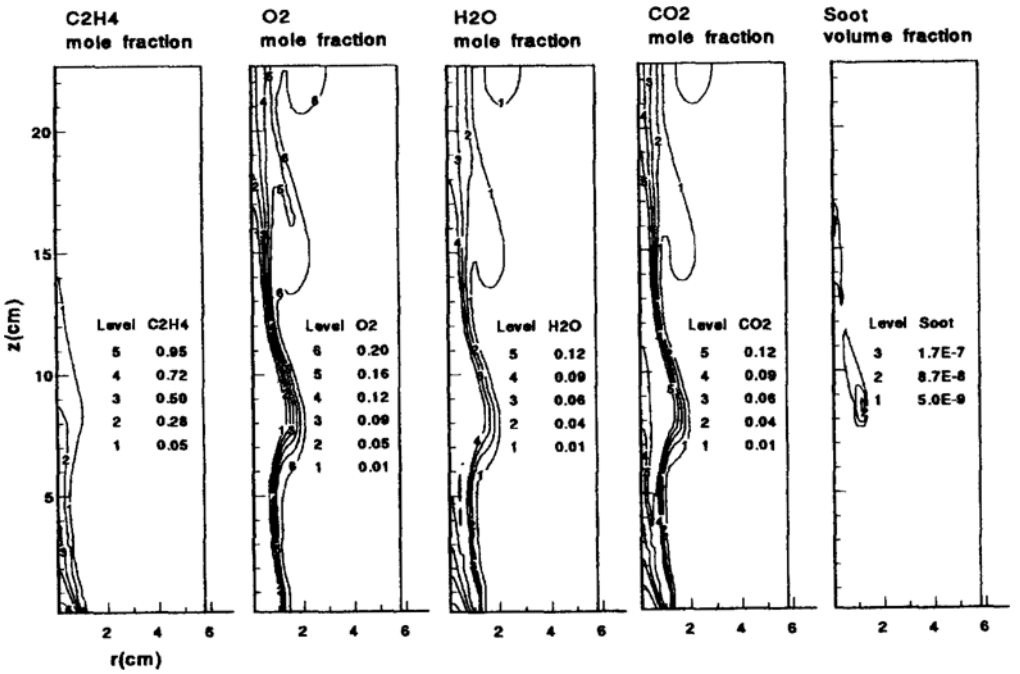

Fig. 7 Instantaneous contours of flame properties at time step 20000 for case of Flame I.

mole fraction profiles are located in the region of high flame temperature where fuel and oxygen meet. Also, soot volume fraction has its maximum value, 3.2×10^{-7}, within the high temperature region.

Radiative quantities are shown in Figure 8.The absorption is emanating primarily from the sooting region, and the region in the flame where $\nabla \cdot q_r$ attains a maximum positive value lies in the same region as the sooting zone. The region of maximum $\nabla \cdot q_r$ corresponds to the region where the energy losses due to radiation are greatest. Figure 8 also shows the radiative heat flux vectors directing outward from the sooting region. From these results, we can expect that soot is the dominant absorbing-emitting medium in the flame.

Two additional simulations were conducted with 0.05m and 0.1m pool diameters to study the scale effects on the nature of these flame oscillations. In both cases, time steps and other conditions are the same as those for the case of Flame I.

The resulting time-sequence of temperature contours for Flame II are shown in figure 9.The time interval between frames is 50ms from 20000 time step. In the first frame, the location of flame bulge is approximately at $z=12$cm. The flame grows and outer vortices move upward in the next frame. In the third frame, a bulge again occur at

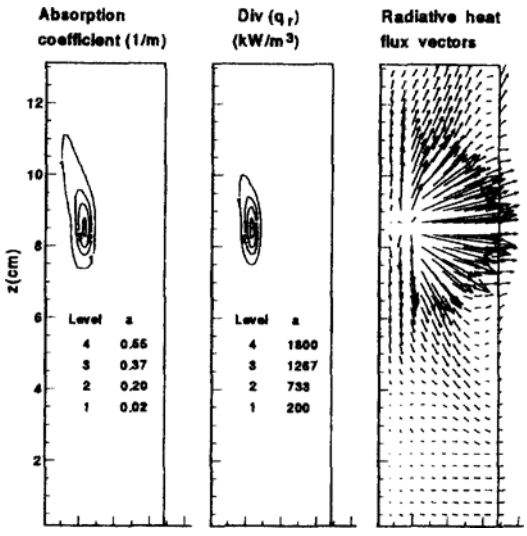

Fig. 8 Instantaneous contours of radiation quantities at time step 20000 for case of Flame I.

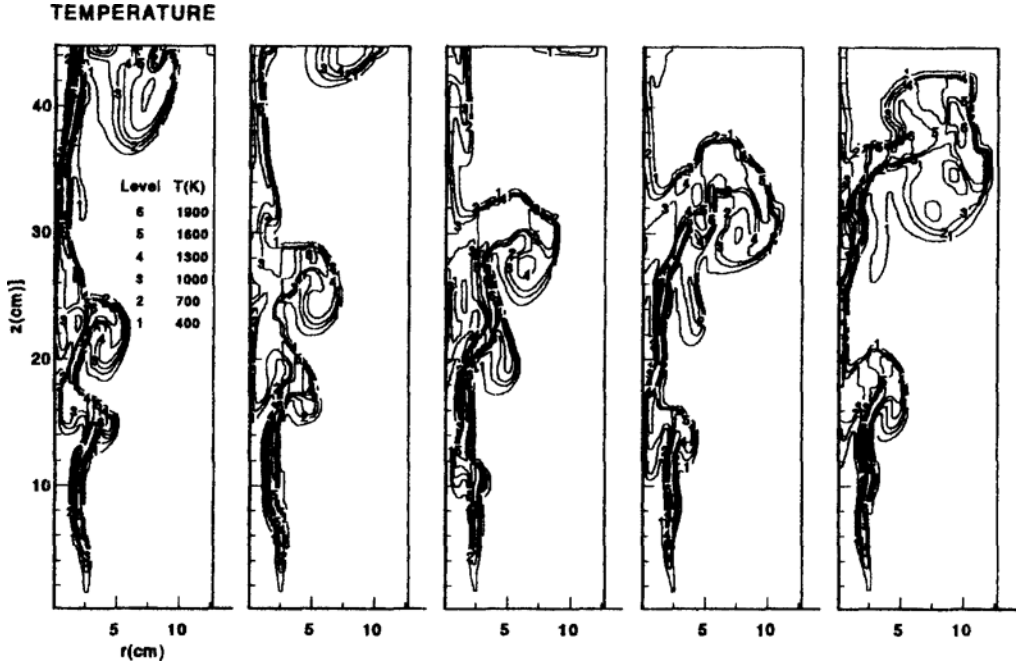

Fig. 9 Time-sequence of selected temperature contours from time step 20000 for case of Flame II. The time interval between frames is 50ms.

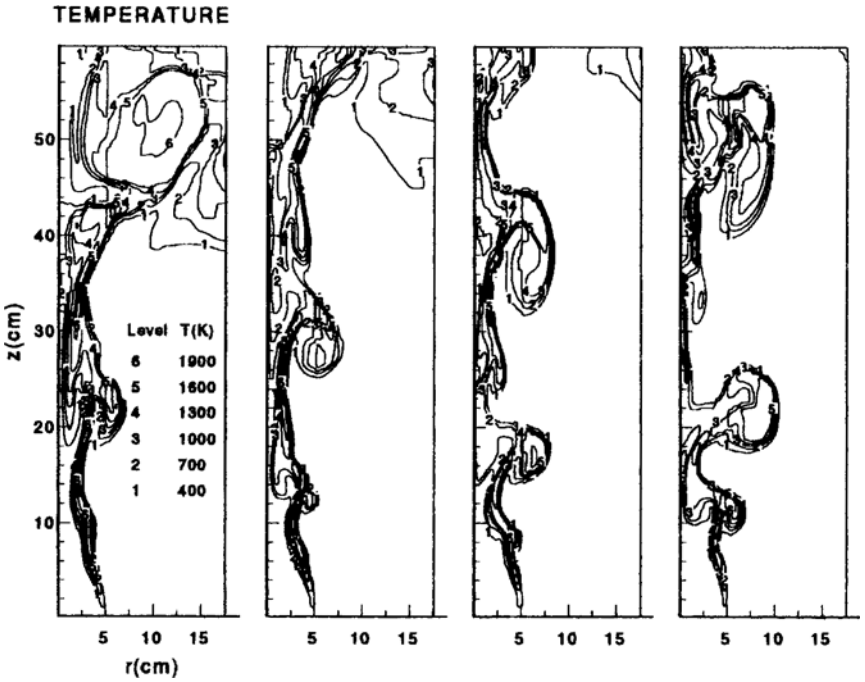

Fig. 10 Time-sequence of selected temperature contours from time step 24000 for case of Flame III. The time interval between frames is 80ms.

the base of the flame, and at the next stage, it locates at a similar position as in the first frame. These steps repeat to give the present flame the oscillation frequency with a range of 6-7Hz, which agrees well with the experimental result of 6.8Hz of same size (see Fig. 1).

Figure 10 shows the time-sequence of the temperature contours for Flame III. The time interval between frames is 80ms. As diameters are larger, the flame becomes more irregular and the formation and movement of the instabilities are more random processes. Therefore, determination of its frequency is not easy compared to the cases of Flame I and Flame II. In the view of the location of flame bulge, however, we can estimate its repeating frequency to be in the range of 4-5Hz, and from Fig. 1, the dominant oscillation frequency of pool diameter D=10cm is 4.8Hz.

5. Conclusion

We have tried to describe the physics involved in freely burning pool fires in considerable detail. First, the numerical results are validated by comparison with experimental data for a low speed diffusion flame, and then the fires above 0.02m, 0.05m and 0.1m circular pools of ethylene have been studied numerically. The computations have been shown to predict the correct qualitative features of pool fires.

The velocity profiles show the action of the strong buoyancy forces which rapidly accelerate the gas flow along the flame axis. The magnitude of the centerline axial velocity near the combustion height is approximately two order greater than the initial velocity at the burner exit. The maximum flame temperature is located in the region where H_2O and CO_2 mole fractions are maximum. The sooting region is located within the high temperature region and as expected, the soot is proved to be the dominant absorbing-emitting medium in the flame.

In pool fires, the source diameter affects the flow dynamics. The model developed is capable of predicting the scale effects and revels trend similar to what has been observed by earlier investigators. Especially, the periodic formation of large-scale structures is clearly visible and its

oscillation frequency agrees well with the data which have been reported in previous investigation of fires of similar sizes.

References

Go Su Yang and Ian M. Kennedy, 1995, "Soot Measurement in a Chlorinated Counterflow Diffusion Flame Using a Laser Scattering and Extinction Technique," KSME International Journal, Vol. 9, No. 3, pp. 369~376.

Kent, J. H. and Honnery, D. R., 1990, "A Soot Formation Rate Map for a Laminar Ethylene Diffusion Flame," *Combust. Flame,* Vol. 79, pp. 287~298.

Kwangsoon Ha and Sangmin Choi, 1994, "Interpretation of Emission Image of an Axisymmetric Diffusion Flame into 2-Dimensional Temperature Data Using a Simplified Computed Tomography," KSME International Journal, Vol. 8, No. 1, pp. 94~102.

Magnussen, B. F. and Hjertager, B. H., 1977, "On Mathematical Modeling of Turbulent Combustion with Special Emphasis on Soot Formation and Combustion," *Sixteenth Symposium (Int.) on Combustion,* pp. 719~729.

Moss, J. B., Stewart, C. D. and Syed, K. J., 1988, "Flowfield Modelling of Soot Formation at Elevated Pressure," *Twenty Second Symposium (Int.) on Combustion,* pp. 413~423.

Nagle, J. and Strickland-Constable, R. F., 1962, *Proceedings of the Fifth Carbon Conference, Pergamon,* New York, Vol. 1, p. 154.

Patnaik, G., Guirguis, R. H., Boris, J. P. and Oran, E. S., 1987, "A Barely Implicit Correction for Flux Corrected Transport," *J. Comput. Phys.,* Vol. 71, p. 1.